Supplementary Information for

Chiral discotic derivatives of 1,3,5-triphenyl-6-oxoverdazyl radical

Aleksandra Jankowiak,[a] Damian Pociecha,[b] Jacek Szczytko,[c] and Piotr Kaszynski* [a,d]

[a] *Department of Chemistry, Vanderbilt University, Nashville, TN 37235, USA, Tel: 1-615-322-3458; E-mail: piotr.kaszynski@vanderbilt.edu.*
[b] *Department of Chemistry, University of Warsaw, Żwirki i Wigury 101, 02-089 Warsaw, Poland*
[c] *Institute of Experimental Physics, Faculty of Physics, University of Warsaw, Hoża 69, 00-681 Warsaw, Poland*
[d] *Faculty of Chemistry, University of Łódź, Tamka 12, 91403 Łódź, Poland.*

Table of Content:

1. Additional photomicrographs

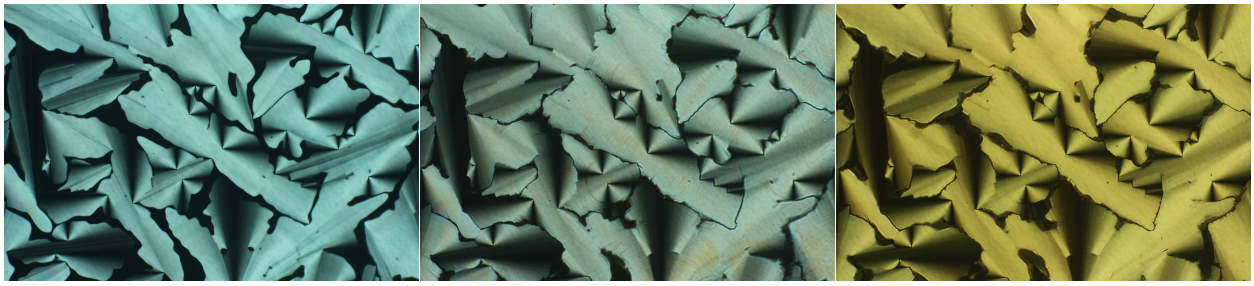

a) T = 77 ºC b) T = 59 ºC c) T = 55 ºC

Fig. S1. Optical textures obtained for **1c** on cooling showing a) Col_h phase, b) $Col_h \rightarrow Col_{h(o)}$ transition, and c) $Col_{h(o)}$ phase. No top cover slide.

a) T = 68 ºC a) T = 58 ºC

Fig. S2. Optical textures obtained for **1c** on cooling in a planar 5 μm cell showing a) Col_h phase and b) $Col_{h(o)}$

2. Powder XRD measurements

X-ray diffraction experiments in broad angle range were performed with Bruker D8 GADDS (Cu Kα radiation, Göbel mirror, point collimator, Vantec 2000 area detector) equipped with a modified Linkam heating stage. For small angle diffraction experiments Bruker Nanostar system was used (Cu Kα radiation, cross-coupled Göbel mirrors, three pinehole collimation, Vantec 2000 area detector). Samples were prepared in a form of a thin film or a droplet on heated surface. The X-ray beam was incident nearly parallel to sample surface. Results are shown in Fig. S3 – S8 and Tables S1 and S2.

Small angle XRD patterns recorded as a function of temperature showed that the

lattice parameters were only weakly temperature dependent in both Col_h and $Col_{h(o)}$ phases (Fig. S3).

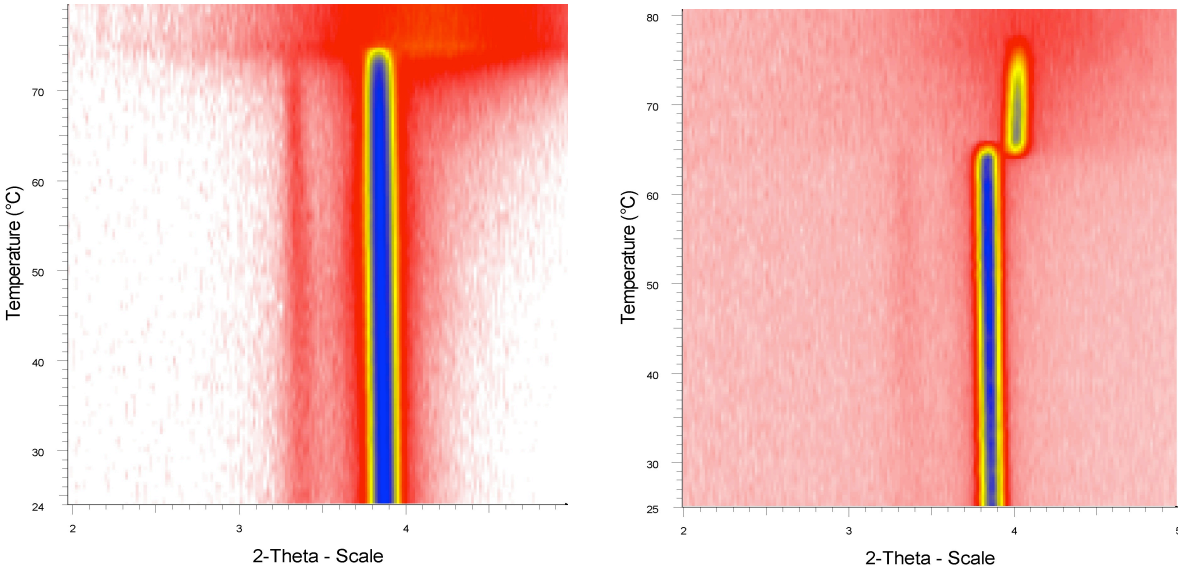

a) b)

Fig. S3. Temperature dependence of the position of low angle reflections for **1b** (a) and **1c** (b) recorded on heating. Intensity (logarithmic scale) is color-coded (white <red < yellow < blue). The weak lowest angle reflection, visible for Col_{ho} phase of both compounds, appears due to doubling of the basic hexagonal structure.

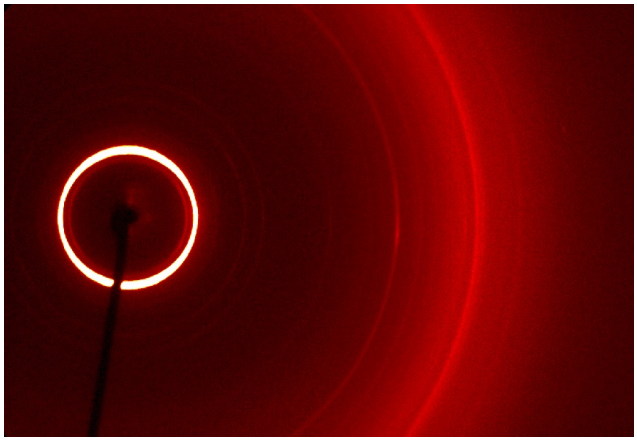

Fig. S4. 2D XRD pattern in broad angle range obtained for powder sample of **1b** at 60 °C. Number of sharp reflections over entire angular range demonstrates that the structure is highly ordered, however in the wide angle range a broad background signal is visible, pointing to a disordered (liquid-like) state of the terminal chains. The pattern can be indexed assuming $Col_{h(o)}$ phase structure: 2D lattice of columns with long-range correlations of molecular distances along column axis.

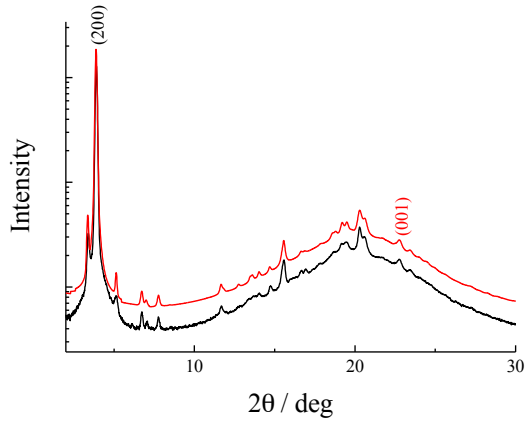

Fig. S5. XRD pattern for **1b** at 30 °C, measured (black) and simulated (red) assuming 2D lattice with hexagonal symmetry and unit cell parameter a = 52.6 Å. The only sharp signal, which does not match the assumed 2D model is indexed as (001) and attributed to molecular positions correlations along columns.

Table S1. X-ray diffraction data for **1b** at 60 ºC. Indexing assuming hexagonal lattice with doubled a parameter (with respect to the molecular diameter) and the unit cell containing 4 molecules.[a]

Phase	Miller indices *h k l*	d_{meas} /Å	d_{calcd} /Å	Cell parameters /Å
$Col_{h(o)}$	1 1 0	26.15	26.30	a = 52.60
	2 0 0	22.78^{m}	22.78	c = 4.38
	2 1 0	17.23	17.22	
	2 2 0	13.17	13.15	
	3 1 0	12.56	12.64	
	4 0 0	11.40	11.39	
	6 0 0	7.58	7.59	
	6 1 0	6.94	6.95	
	6 2 0	6.32	6.32	
	7 1 0	6.02	6.03	
	8 0 0	5.70	5.69	
	8 1 0	5.33	5.33	
	6 4 0	5.24	5.23	
	9 1 0	4.76	4.77	
	10 0 0	4.55	4.55	
	0 0 1	4.38	4.38	
		4.4^{diff}		

[a] Index *m* denotes the main diffraction signal, index *diff* denotes the broad (diffused) signal.

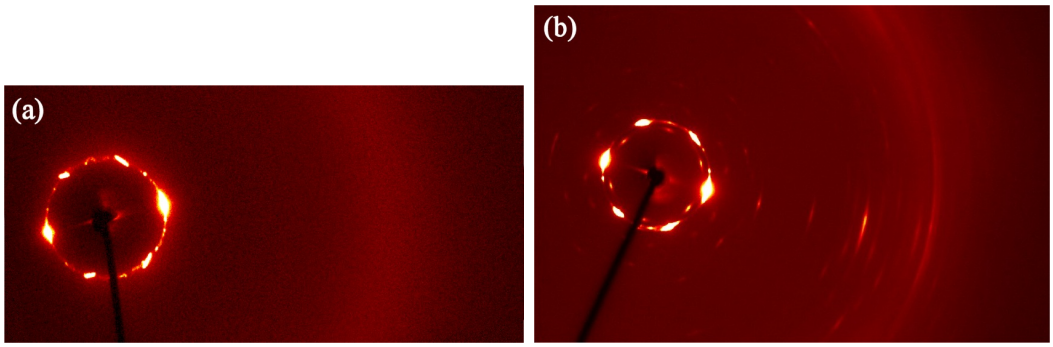

Fig. S6. 2D XRD patterns in broad angle range obtained for aligned sample of **1c** at (a) 75 °C, *Col*$_h$ phase, and (b) 30 °C, *Col*$_{h(o)}$ phase.

Table S2. X-ray diffraction data for **1c**. Indexing was done assuming hexagonal crystallographic lattice, in *Col*$_{h(o)}$ phase the lattice parameter *a* is doubled with respect to the *Col*$_h$ phase.[a]

Phase	Miller indices *h k l*	d_{meas} /Å	d_{calcd} /Å	Cell parameters /Å
Col$_h$ T = 75 °C	1 0 0	21.70^m	21.70	a = 21.70
		4.6^{diff}		
Col$_{h(o)}$ T = 75 °C	1 1 0	26.10	26.26	a = 52.52
	2 0 0	22.71^m	22.74	c = 4.36
	2 1 0	17.16	17.19	
	2 2 0	13.12	13.13	
	4 0 0	11.37	11.37	
	6 0 0	7.58	7.58	
	6 2 0	6.31	6.31	
	7 1 0	6.01	6.02	
	8 0 0	5.69	5.68	
	8 1 0	5.32	5.32	
	6 4 0	5.22	5.25	
	8 2 0	4.97	4.96	
	10 0 0	4.55	4.55	
	0 0 1	4.36	4.36	
		4.4^{diff}		

[a] Index *m* denotes the main diffraction signal, index *diff* denotes the broad (diffused) signal.

In ordered columnar hexagonal phases of **1b** and **1c** derivatives it was observed that the crystallographic lattice parameter is doubled with respect to the one observed in disordered type phase of **1c** (which means it is comparable to twice the molecular diameter).

The unit cell of enlarged lattice contains 4 molecules. The lattice doubling manifested by te apperance of additional diffraction signals, some of them being subharmonics of the signal observable for basic lattice (Fig. S7). Interestingly, there was no subharmonic of the strongest signal (indexed as *10* in basic lattice), while the subharmonic of (*11*) signal did appeare.

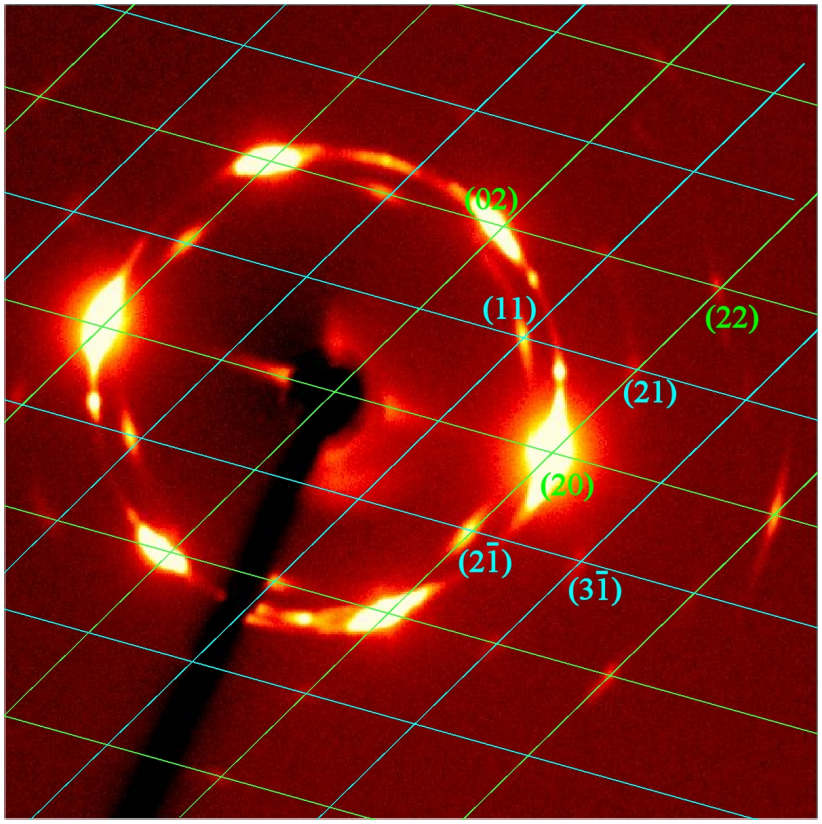

Fig. S7. 2D XRD patterns in small angle range obtained for aligned sample of **1c** at 30 °C, $Col_{h(o)}$ phase. Green lines represent the reciprocal lattice related to the basic hexagonal structure of the columns. Note that the most intense signals (marked in green) can be indexed to this lattice. In blue there are additional lines, which appear due to new structure with doubled periodicity, superimposed on the basic one. All the indexes given are related to enlarged lattice. Signals marked with blue indexes are due to superstructure, their relatively low intensity indicates that additional superstructure only weakly influences the main electron density modulations related to arrangement of molecules into columns. Interestingly, the signals (*10*), which are typically the strongest ones for hexagonal lattice, are absent.

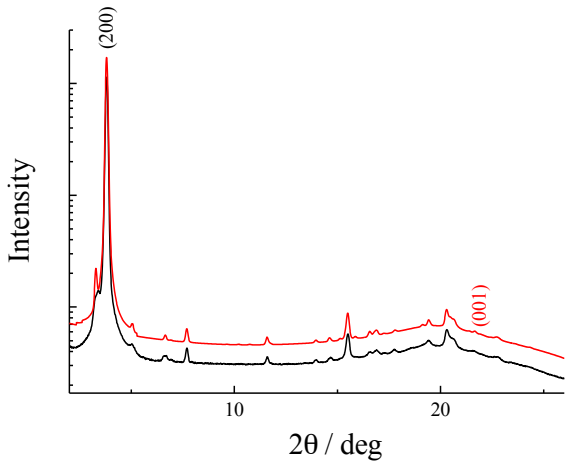

Fig S8. XRD pattern for **1c** at 30 °C, measured (black) and simulated (red) assuming 2D lattice with hexagonal symmetry and unit cell parameter a = 52.5 Å. The only sharp signal, which does not match the assumed model is indexed as (001) and attributed to molecular positions correlations along columns.

3. Magnetization measurements

Experiments were conducted using SQUID magnetometer (Quantum Design MPMS-XL-7T).

A fresh sample of **1c** (m = 21.13 mg, 13.50×10^{-6} mol, M_w=1565.43) was placed in a polycarbonate capsule fitted in a plastic straw. The sample was subjected to heating and cooling experiments at 200 Oe in a range of temperatures of between 2 K and 370 K at a rate of 1 K min^{-1}. The total molar suscebility of the sample χ in the full temperature range is shown in Fig. S9.

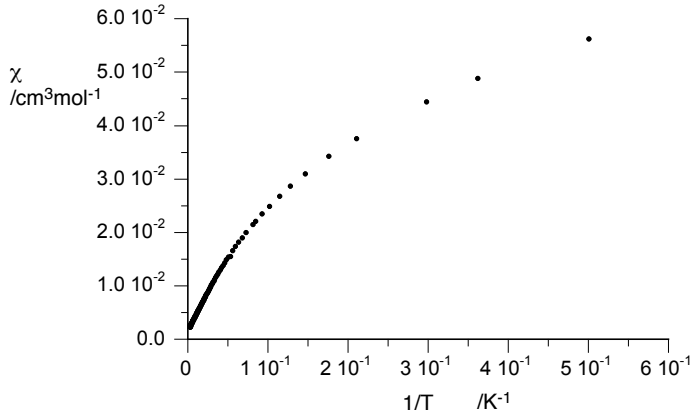

Fig. S9. Molar magnetic susceptibility χ of **1c** vrs 1/T in a range of 2 K–370 K obtained on cooling at 200 Oe. Cooling rate 1 K/min.

The correction for diamagnetic and impurity contributions was established by analysis of the high temperature magnetization data obtained on cooling (Fig. S10). It was assumed that **1c** is a pure paramagnet in the iostropic phase and obeys the Curie-Weiss law (eq 1). The Weiss constant θ was fitted in such a way that the Curie constant is close to the ideal value of 0.375. Thus, setting θ = –4 K, the fitting gave C = 0.376(19) and correction χ_{corr} = 0.00136(5).

$$\chi_m = \frac{C}{T-\Theta} \quad \text{(eq 1)}$$

The value θ established from the Curie-Weiss law fitting is consistent with results of analysis high field (H > 0.1 T) magnetization data with a modified Brillouin function $\mathcal{B}\left(B, T+\theta, S=\frac{1}{2}\right)$.

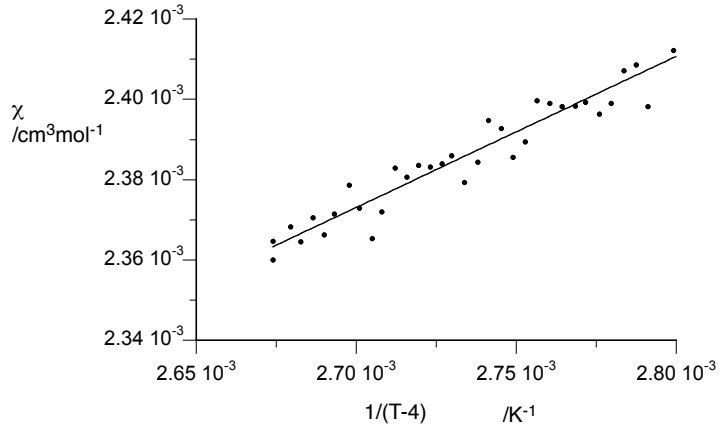

Fig. S10. Molar magnetic susceptibility χ of **1c** vrs 1/T in a range of 353 K–370 K obtained on cooling and heating at 200 Oe. Best fit line: χ = 0.376/(T-4) + 0.00136; r = 0.96.

The correction value χ_{corr} was substracted from the total molar suscebility (χ) giving molar paramagnetic suscebility, χ_p. A plot of χ_p vrs 1/(T-θ) is shown in Fig. S11. The molar susceptibility χ_p was converted to dimensionalless μ_{eff} according to the equation $\mu_{eff} = 2.828 \bullet (\chi_m T)^{1/2}$ (Hoppeè, J. I. *J. Chem. Ed*. **1972**, *49*, 505).

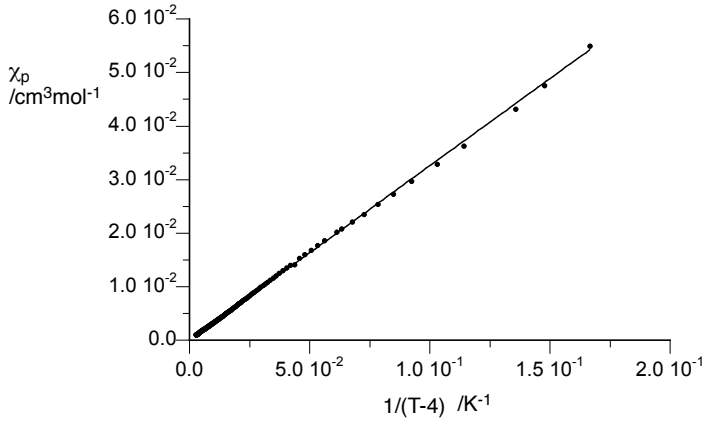

Fig. S11. Molar paramagnetic suscebility (χ_p) vrs 1/(T-4) recorded on cooling at 200 Oe. Range 2 K– 370 K. Best fit line: $\chi = 0.325/(T-4)$; $r^2 = 0.999$.

Histeresis of the magnetic transition is demonstrated for **1c** in Fig. S12.

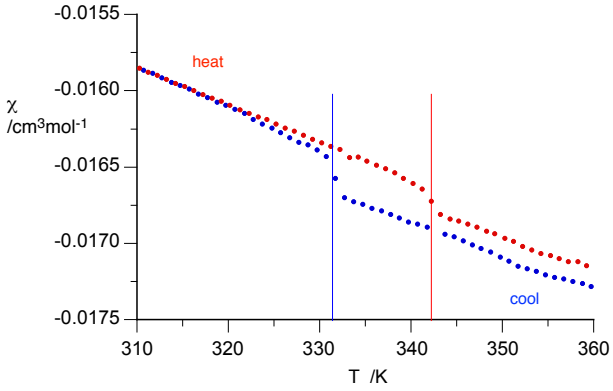

Fig. S12. Molar magnetic susceptibility χ of **1c** vrs T in a range of 310 K–360 K obtained on cooling (blue) and heating (red) at 7 T. The vertical line marks the Col_h –$Col_{h(o)}$ phase transitions.